Influence of Lateral Confinement on Phase Separation in Thin Film Polymer Blends

Bi-min Zhang Newby* and Russell J. Composto

Department of Materials Science and Engineering and Laboratory for Research on the Structure of Matter, University of Pennsylvania, Philadelphia, Pennsylvania 19104

Received December 14, 1999; Revised Manuscript Received February 22, 2000

ABSTRACT: Thin films of polymer blends are molded into strips for investigating the influence of lateral confinement on phase separation. The strip has a width and thickness of 17 μm and 1.0 μm, respectively, and contains a 50/50 blend of poly(methyl methacrylate) (PMMA) and poly(styrene-*ran*-acrylonitrile) (SAN). Upon annealing, the strip profile rapidly becomes bell-shaped, forming a contact angle of 3° with the substrate. The dynamics of phase separation is investigated using confocal microscopy and atomic force microscopy. The early stage is characterized by an interconnected morphology and symmetric wetting of the PMMA-rich phase at the substrate and surface. The PMMA-rich domains grow from the surface toward the substrate during the early intermediate stage and eventually connect with the wetting layer covering the substrate to begin the late intermediate stage. The domain diameter increases rapidly (early), slows down (intermediate), and then decreases (late) during phase separation. During the late stage the PMMA-rich domains heal, leaving behind an elliptical SAN-rich core encapsulated by PMMA-rich wetting layers. These studies demonstrate that confinement directs the formation of a self-assembled core/shell morphology, which has potential applications for encapsulating drugs or creating microwires.

Introduction

Polymer blend thin films have received much attention by both experimentalists[1−10] and theorists[11−18] in recent years. This interest has been motivated partly by their commercial applications such as adhesives, photoresists, and more recently biopatterned surfaces. Fundamental studies have mainly focused on how the presence of a surface alters the dynamics of phase separation in polymeric films. For example, surface effects have been observed to produce composition fluctuations perpendicular to the film surface, a phenomenon called surface directed spinodal decomposition. In addition, Tanaka[19,20] studied the interplay between wetting and phase separation in thin film mixtures confined between hard walls. Moreover, phase growth in thin films is perturbed relative to the bulk because of broken symmetry due to confinement.[2,3] However, lateral confinement studies have mainly been limited to phase separation in capillary tubes (i.e., hard walls). Only recently, by employing advances in soft lithography techniques,[21] polymer blend thin films can be molded into uniform and narrow (10−100 μm) strips on solid substrates. The purpose of this paper is to explore the dynamics of phase separation of polymer blends in such a laterally confined strip.

Recently, phase separation studies have been performed on polymer thin films on substrates having stripes with alternating surface interactions.[22−25] Upon spin-casting unstable blends in solution, the two domains are directed onto the different stripes. In contrast to these studies on patterned surfaces, we first guide both components to the same confined region and then investigate the dynamics of phase separation. Such confinement will influence the final structure, which depends on the surface energy and viscosity of each component as well as the polymer/polymer and polymer/substrate interfacial energies. This structure also depends on the wetting properties. For symmetric wetting, where one phase prefers both the surface and substrate, an ellipse-like core of one phase will be encapsulated by the other phase as shown in Figure 1. We will demonstrate that lateral confinement directs phase separation to produce this stable core−shell structure, in striking contrast to the behavior of semiinfinite films.

Semiinfinite films of poly(methyl methacrylate) (PMMA) and poly(styrene-*ran*-acrylonitrile) (SAN) at a critical composition were previously investigated.[26−28] For thin films on an oxide substrate, the PMMA-rich phase rapidly wets both the surface (vacuum) and substrate (i.e., symmetric wetting). These wetting layers are fed by an adjacent bicontinuous structure through which the PMMA flows. As PMMA-rich domains grow in the SAN-rich interphase, a trilayer, PMMA-rich/SAN-rich/PMMA-rich, structure parallel to the surface develops. Because of capillary fluctuations, the SAN-rich layer eventually ruptures, and the entire film undergoes macroscopic roughening. One question to consider is how lateral confinement would influence the evolution of phase separation and the final morphology.

In this paper, we confine PMMA:SAN blends to narrow strips (∼20 μm) and follow the dynamics of phase separation. Using AFM and confocal microscopy, we identify and quantify the stages of phase evolution by measuring the number density of PMMA-rich domains, the domain size, and the wetting layer thickness. To our knowledge, this is the first quantitative study of phase separating polymer blends in a laterally confined geometry with a free surface. The phase separation is divided into early, intermediate, and late stages. Similar to the semiinfinite film case, symmetric wetting occurs simultaneous with internal phase separation. The wetting layer thickness along the center of the strip increases dramatically during the early stage, decreases slowly during the intermediate stage, and approaches a constant value during the late stage. The PMMA-rich domains inside the SAN-rich matrix also

* Corresponding author.

10.1021/ma992092m CCC: $19.00 © 2000 American Chemical Society
Published on Web 04/12/2000

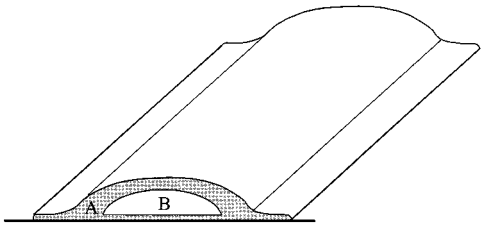

Figure 1. This cartoon illustrates one possible morphology of a polymer blend which has undergone simultaneous phase separation and wetting with lateral confinement. The symmetric wetting of the A-rich phase dominates the phase morphology resulting in a B-rich core encapsulated by an A-rich shell.

grow rapidly, by hydrodynamic flow, during the early stage. These domains continue to grow by diffusion and coarsening during the intermediate stage to a maximum value and then heal during the late stage. In contrast to the semiinfinite film, the SAN-rich phase is stable and forms an ellipse-like core encapsulated by PMMA-rich wetting layers. The stability of this core/shell structure is consistent with the theory of a capillary thread inside a liquid medium.

Experimental Section

Materials. The polymer system is a blend of poly(methyl methacrylate) (PMMA) and poly(styrene-*ran*-acrylonitrile) (SAN). The PMMA, purchased from Polymer Sources Inc., has a weight-average molecular weight of 91 000 and a polydispersity index of 1.03. The polymer was prepared by anionic polymerization in tetrahydrofuran. This polymer was used as purchased without further purification. The SAN, obtained from Solutia Inc., contains 33 wt % of AN and has a weight-average molecular weight of 118 000 and a polydispersity index of 2.24. The SAN was purified by pouring a solution of SAN and chloroform into a large volume (10:1) of methanol. After allowing the SAN to precipitate for 1 h, the methanol was removed, and the precipitant was scooped out and placed in a watch glass. The wet precipitant, loosely covered by aluminum foil, was first dried under ambient conditions for at least 6 h and then inside a vacuum oven at 80 °C for 16 h. The dried SAN was then redissolved in chloroform and precipitated two more times. The glass transition temperatures of PMMA and the purified SAN measured with a differential scanning calorimeter at a heating rate of 20 °C/min are 126 and 115 °C, respectively.

The phase diagram was determined from thin films (10−20 μm) of the PMMA/SAN blend. These thin film blends were deposited onto glass slides and annealed in a vacuum oven at temperatures ranging form 153 to 215 °C. The cloud point was defined as the temperature at which the film, viewed against a black background, changed from transparent to opaque. Figure 2 shows that PMMA/SAN displays a lower critical solution temperature or LCST with a critical temperature of 160 °C. The LCST behavior is consistent with previous experiments.[29−33] Near the critical temperature, the phase diagram is relatively flat between 25 and 75 wt % of PMMA and increases sharply below 20 wt % and above 80 wt %. Above 175 °C, SAN is more miscible in PMMA than vice versa. For this paper, a 50 wt % blend is annealed at 200 °C in a vacuum oven. Thus, the equilibrium concentrations for the SAN-rich and PMMA-rich phases are around 4 and 92 wt % of PMMA, respectively.

Sample Preparation. Thin films of polymer blends were confined into microsized (~20 μm) strips using micromolding from solution (MIMS). MIMS is a modification of the micromolding in capillaries technique developed by Xia and Whitesides.[21] Other techniques, such as microcontact printing, microtransfer molding, and micromolding in capillaries, are either incapable of generating polymer strips with a thickness greater than 1 μm and a length of more than 50 μm or unable

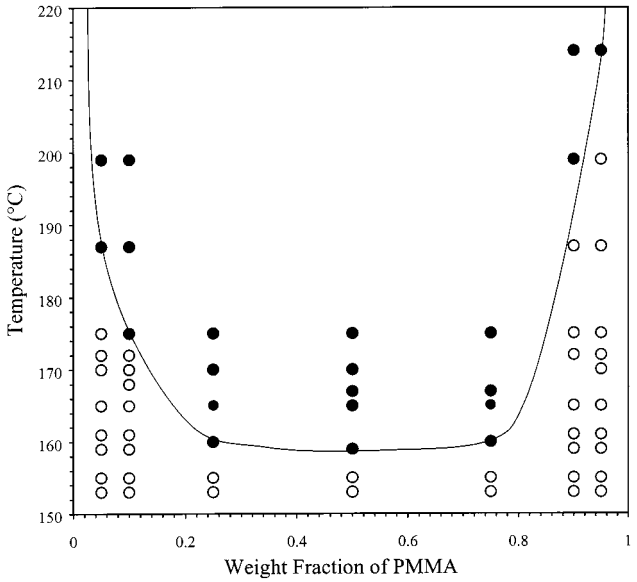

Figure 2. Phase diagram of a PMMA/SAN blend shows a lower critical solution temperature behavior with a critical temperature of ca. 160 °C. The filled circles represent two-phase blends (i.e., opaque), whereas the open circles are transparent after 1 week at the annealing temperature. In this paper, experiments are performed at 200 °C where the coexisiting compositions are approximately 4% and 92% of PMMA for the SAN-rich and PMMA-rich phases, respectively. The solid line is a guide to the eye.

to consistently create large regions with clean spacing between the strips. In MIMS, a micromold was used to generate the microsized strips onto a substrate. The micromold was a patterned elastomer of poly(dimethylsiloxane) (PDMS). The PDMS was used as a mold because of its good flexibility, excellent release properties, and ability to accurately capture the pattern from the master mold. The details of mold fabrication can be found in ref 21. The mold in this study contained 125 rectangular channels with a height, width, and length of 1.4 μm, 15 μm, and 500 μm, respectively. The spacing between the channels was 25 μm. The substrate was a 1 cm × 1 cm silicon wafer cleaned with a piranha solution and stored under DI water prior to use. The polymer solution was 5 wt % of 50/50 PMMA/SAN by mass (or 48/52 PMMA/SAN by volume) dissolved in methyl isobutyl ketone (MIBK). During molding, a drop of filtered (0.45 μm Teflon filter from Fisher) solution was first deposited on the silicon substrate, which was placed on the hot plate at 60 °C. The solution was allowed to concentrate into a viscous but flowable liquid (the exact concentration of the liquid was unknown) upon solvent evaporation. Then, the micromold was pressed onto the solution and held in place with some pressure until most solvent evaporates and the strips solidify. Then, the mold was gently removed. The samples were then placed in a vacuum oven at 110 °C for 16 h to remove any remaining solvent. Prior to annealing, the dimensions of the strips were determined by AFM. Then, samples were annealed under vacuum (35 μmHg) at 200 °C for various times, and their phase morphologies were evaluated.

Imaging. The phase morphologies were examined by tapping mode atomic force microscopy (AFM, DI multimode) and confocal laser scanning microscopy (Leica optical microscope combined with a confocal head from Noran Instruments). The confocal images were taken with a reflected laser beam, and each image contained an average of 32 scans. The confocal microscope images were taken over an area of 67 μm × 63 μm. From this area, a small portion (20 μm × 20 μm) was selected for viewing. The number density and phase shape were qualitatively evaluated by confocal microscopy, whereas quantitative analysis was performed using AFM.

To quantify phase evolution, AFM was used to determine the topography of at least three strips at a particular time.

The image size was 22 μm × 22 μm or 24 μm × 24 μm. The AFM scan rate was 0.5 Hz, and the set point was close to 2 V. To reveal the phase morphology, the PMMA-rich phase was selectively etched by first irradiating with 2.0 MeV He^{2+} ions at a dose of 2 μC followed by etching in acetic acid for 2 min. The same area was scanned by AFM before and after etching. Using AFM analysis in this way, we were able to determine the PMMA-rich phase number density, diameter, shape, and depth as well as the wetting layer thickness and final morphology. Because domain shape near the growth front plays an important role, the limitations of AFM for evaluating narrow features should be presented.

The atomic force microscope has some physical limitations due to finite tip size when imaging narrow and steep features. The tip is an etched silicon probe (DI model TESPW) with a radius of curvature of 5−10 nm and a height of 12.5 μm. Because the front and back angles of the tip are 25° and 10°, respectively, the maximum angles that can be accurately followed by the tip are 65° and 80°, respectively. Because of this limitation, only a portion of the phase morphology can be detected inside a narrow feature. Also, if a phase has a contact angle greater than 65° or 80° (depending on the direction of scanning) with the substrate, the phase image will be influenced by the tip. Unertl[34] has presented a detailed analysis of tip shape limitation during AFM scanning.

Key Parameters and Their Measurement. The confined thin film was defined in terms of its height, width, and contact angle with the substrate. Using the AFM topography, the values for these parameters were determined by measuring five cross sections for each of three strips. Subsequently, the PMMA-rich phase was removed to determine the number density (N_d) of PMMA domains inside the SAN matrix, the diameter (D), correlation length (ξ), and depth (h) of the PMMA domains. For all parameters, the measurements were taken within the center of the strip. During the early stage (1, 2 h) of phase separation, the PMMA domain size was small, and a 5.5 μm × 5.5 μm image was selected from the center of the entire image (22 μm × 22 μm) for analysis. The images were initially black and white contrast enhanced and then analyzed using a Scion image to count the number of PMMA domains. The value of N_d was an average of six measurements. For longer annealing times (4 h to 732 h), the value of N_d was obtained by counting the domains in a 5 μm × 20 μm area along the center of the strip. This value was an average of three measurements.

The values of ξ, D, and h were obtained from AFM cross-sectional analysis. The correlation length was measured from the center of one domain to the other. The diameter was defined as the length from one domain edge to the other through the center of the domain. The depth of the domain was determined by averaging the vertical distances from each edge of the domain to the bottom of the domain. The PMMA wetting layer thickness was given by the difference in height, at the same spot, before and after removing the PMMA phase. Only the wetting layer thickness at the center of the strip was used. The data points in this study represent the average of at least 10 measurements.

Results

Strip Shape and Contact Angle. Before quantifying phase and wetting evolution, the shape of the polymer blend thin film was characterized by AFM. The typical as-molded strip is about 1.0 μm high near the center by 17 μm wide by 200 μm long. The spacing between the strips is ca. 23 μm. In part, the micromolding technique previously described was chosen because it produced strips of rather uniform width along the entire length. Initially, both strip edges are higher than the center region and form a nearly 45° angle with the substrate. Upon annealing at 200 °C (∼80 °C above the glass transition temperatures), the strip cross section quickly (<1 h) relaxes and becomes bell-shaped as shown in Figure 3. By plotting the cross section using the same lateral and height scales, the gradual decrease in film thickness between the center and edge is clearly observed. This shape is maintained throughout the entire phase evolution. To quantify film shape, the contact angle at the polymer/substrate interface was measured over the entire annealing time for a particular strip. The contact angle quickly decreases to 3.5° after 1 h and then slowly approaches a small, yet finite, angle of 3° after 300 h. From AFM and selective etching,[26−28] the PMMA-rich phase is known to encapsulate the nonwetting SAN-rich phase. Furthermore, PMMA is known to wet silicon oxide, which covers the entire surface of the wafer. However, the contact angle never becomes 0° (i.e., complete wetting), providing the first indication that the polymer blend is indeed confined laterally.

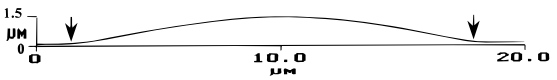

Figure 3. AFM cross section of a blend confined to a width and height of 17 μm and 1.2 μm, respectively, after 1 h at 200 °C. The film thickness is relatively constant (i.e., flat) across the center and tapers off slowly toward the edge to a contact angle of 3.5°. The edges of the strip are denoted by arrows.

Phase Evolution. Using confocal light microscopy (Figure 4) and AFM (Figure 5), the morphology of the phase separating blend was evaluated and found to display three distinct regimes. During the early stage ($0 < t < 2$ h), the results are similar to previous studies for the semiinfinite film case.[26−28] Namely, the PMMA-rich phase wets the outer surface and substrate, and the near-surface forms a bicontinuous interconnected morphology. During the intermediate stage (2 h < t < 400 h), PMMA-rich channels grow from the surface-wetting layer until they reach the substrate. This domain growth was not observed for the semiinfinite case.[26−28] Although the contact angle remains fixed, the edges become enriched with the PMMA-rich phase due to rapid coarsening and flow through the wetting layer. During the late stage (t > 400 h), the PMMA-rich domains heal, resulting in an elliptical SAN-rich core encapsulated by a PMMA-rich shell.

Figure 4 shows selected confocal microscopy images representing the early (1, 2 h), intermediate (4, 8, 20, 100 h), and late (732, 1500 h) stages. Interference fringes along the strip edge result from a gradual decrease in thickness between the middle and edge of the strip, as shown in Figure 3. The images are taken by focusing on the center of the strip, which is large (∼5 μm width) and relatively flat. In the first 2 h, the near-surface region displays an interconnected morphology that coarsens. At 4 h, the interconnected morphology starts to disappear, and the PMMA-rich minority phase forms small isolated domains, which are round when viewed from the top. Between 4 and 100 h, these domains increase in diameter and decrease in number. With further annealing (732 h), the domain size begins to decrease (dotted arrow), and in some cases domains completely heal (solid arrow). At 1500 h, the domains in the center of the strip disappear, resulting in a smooth, flat center region along the strip.

Using AFM after removing PMMA, the phase evolution can be followed in detail. Figure 5 shows selected AFM images (top) after 1, 4, 20, and 732 h of annealing, and the cross sections (bottom) at the locations indicated by solid lines in the images. At 1 h (early stage), the

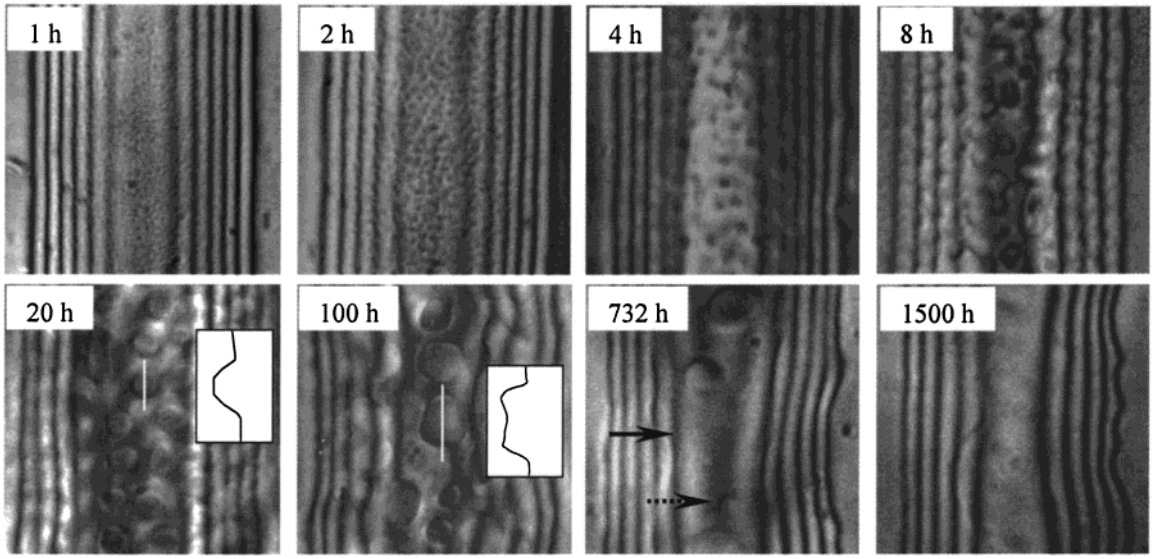

Figure 4. Confocal microscopy images of a 50:50 blend confined to a 17 μm wide strip after annealing at 200 °C. During the early stage (1 and 2 h), a bicontinuous interconnected morphology is observed, whereas the intermediate stage is characterized by isolated domains as shown in the 4 h sample. Domains grow between 4 and 100 h. During the late stage (732 and 1500 h), the domains begin to shrink and heal. The dark and light lines parallel to the edges are interference fringes resulting from the gradual change in film thickness. The images are 20 μm × 20 μm. The insets at 20 and 100 h are AFM cross sections taken along the white line. The dimensions of the inset are 100 nm by 5 μm.

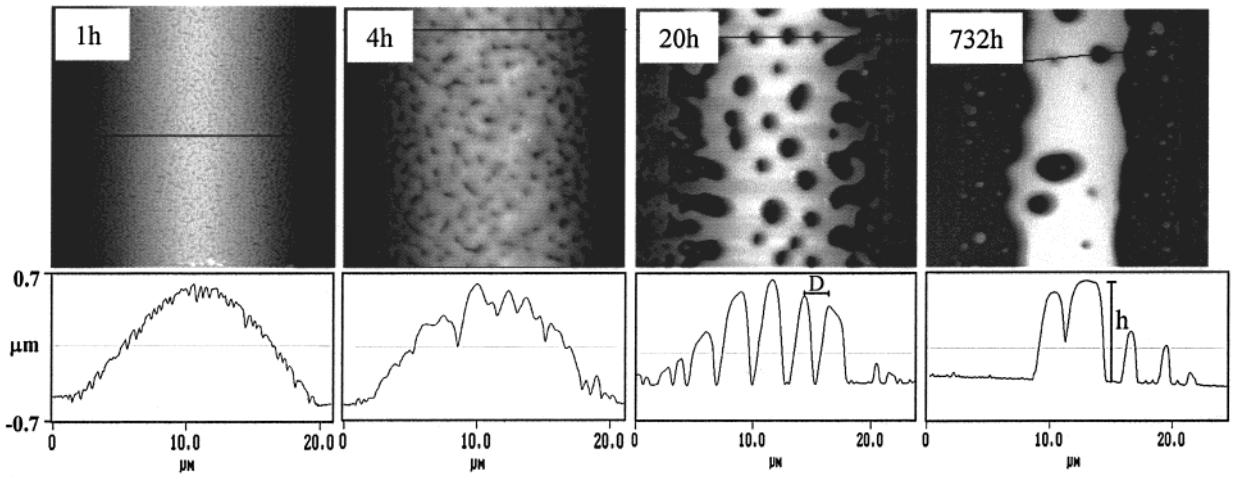

Figure 5. AFM images (top) of the phase morphology after removing the PMMA-rich phase in a confined blend annealed at 200 °C for 1 h (early stage), 4 and 20 h (intermediate stage), and 732 h (late stage). The white (high) strip and dark (low) regions correspond to the SAN-rich phase and the extracted PMMA-rich phase, respectively. The bottom figures show cross sections taken along the black solid lines in the images (top). *D* and *h* are the PMMA-rich domain diameter and depth, respectively. The growth front of the PMMA-rich phase is observed at 1 and 4 h. After 20 h, these phases touch the wetting layer at the substrate and then begin to shrink (732 h). Note that the width of the SAN-rich phase (white) decreases with time.

AFM image shows a bright white (high) center region between the gray edges. The interconnected phase morphology appears uniform across the strip and is particularly apparent near the edge (thin) regions. To quantify phase growth, the height variation from AFM cross-sectional analysis is used. At 1 h, the interface between the PMMA-rich wetting layer and the SAN-rich nonwetting layer is rough. Namely, in addition to growing parallel to the surface as observed in the top view image of Figure 4, the PMMA-rich phases are also penetrating into the SAN-rich matrix below the wetting layer.

During the early intermediate stage (e.g., 4 h), the AFM image shows that the originally bicontinuous morphology has transformed into round PMMA-rich phases (dark) imbedded in the SAN-rich matrix (light). Note that the number density of PMMA-rich phases is much greater near the strip edges compared to the center region. The height variation at 4 h shows that the PMMA-rich phases grow wider and penetrate deeper into the SAN matrix compared to the 1 h case. The SAN-rich phase is found across the entire strip. After 20 h (late intermediate stage), the PMMA-rich phases have penetrated the entire SAN matrix and span the PMMA-rich surface and substrate wetting layers. At 20 h the number density is also lower and phase diameter greater than at earlier times. The strip edges are now mainly the PMMA-rich phase (dark). This image provides direct evidence that the PMMA-rich phase is flowing toward the strip edge. The lateral interfacial area between the central SAN-rich phase and the PMMA-rich phase along the edges is quite large. The gray regions along the left and right edges represent the SAN-rich phase produced by phase separation of thin (∼100 nm) films that are occasionally left over from the molding process.[35]

At 732 h (late stage), the AFM image shows that the number of PMMA-rich phases is greatly reduced because of both phase coarsening and healing of individual PMMA phases. In the later case, three partially healed phases are observed in the top image. Cross-section analysis (bottom) shows that one of these phases only penetrates ca. 500 nm into the SAN-rich matrix. One of the most fascinating observations from this image is the formation of a SAN-rich core (white) encapsulated by PMMA-rich wetting layers. The small round white features near the edges correspond to residual SAN droplets. After 1500 h (not shown), the PMMA-rich domains are further squeezed out of the SAN-rich matrix. On the basis of the lateral area and height at 1500 h, the SAN volume fraction in the center region is about 0.50, close to the initial concentration of the blend.

Throughout phase separation, the PMMA-rich phase flows along the wetting layer and toward the edge of the strip. Initially, a thin PMMA-rich region forms at the outermost edge of the strip and grows toward the center region with time. As the PMMA phase accumulates near the edge, an interface forms between the PMMA-rich outer region and the SAN-rich inner region. Because of PMMA phase coarsening near the edges, this interface is initially very tortuous with a high interfacial area as shown in Figure 5 at 20 h. The lateral interface eventually decreases its area to minimize interfacial energy, resulting in a smooth, well-defined SAN-rich core as shown in Figure 5 at 732 h.

Discussion

Shape and Contact Angle. As shown in Figure 3, the cross section of the polymer blend displays a relatively flat central region, 1.2 μm in height, which gradually decreases in thickness as demonstrated by the equally spaced interference fringes in Figure 4. In this section, the cross-sectional shape caused by the lateral confinement will be discussed. A zero contact angle would be expected if the PMMA wetting layer were allowed to flow freely on the silicon oxide substrate. However, a finite contact angle of 3° is measured which suggests that the PMMA-rich wetting layer is pinned at the PMMA/air /oxide interface. One possible explanation for pinning could be that the substrate between strips has a low surface energy. In the micromolding technique a PDMS elastomer mold, containing square channels, is pressed onto a silicon wafer with an oxide layer. During molding, a thin PDMS layer may transfer onto the silicon oxide surface and reduce the surface energy between strips. We verified the formation of the thin PDMS layer by measuring the contact angle of water after pressing the PDMS mold on the substrate. This angle is about 75°, which is much greater than the value for water on silicon oxide. The transfer of PDMS chains from a PDMS mold to a pressure sensitive adhesive has been observed.[36] Using Young's equation and a contact angle of 3°, the surface energy of the substrate between strips is about 29 mJ/m^2, which is between the surface energy of PDMS (γ = 22 mJ/m^2) and silicon oxide (γ^d = 36.5 mJ/m^2).[37] Thus, lateral confinement of the polymer strip is likely due to the presence of PDMS on the substrate between strips.

A striking result of this study is the formation of a bell-shaped strip enclosing an elliptical SAN-rich core encapsulated by a PMMA-rich wetting layer. To understand why this morphology is stable, we compare the free energy of the experimental cross-sectional profile with a hypothetical profile having a cylindrical core. In both cases, the PMMA volume fraction is 0.48 and the total volume is fixed. For the experimental configuration, a curve is fit to the cross section to estimate the surface area of PMMA. The interfacial area of PMMA/SAN is determined from the cross section after PMMA is removed. For a cylindrical core, the surface area of PMMA would be about 5% larger than the experimental value. On the other hand, the experimental PMMA/SAN interfacial area is almost double that of the cylindrical core. Because the PMMA/SAN interfacial energy[38] ($\sim$0.5 mJ/m^2) is much smaller than the surface energy of PMMA[39] (27.4 mJ/m^2) at 200 °C, the surface area of the wetting layer dominates the system free energy and strongly influences the final shape of strip. By fixing the strip height, strip width, and blend composition, the total free energy of the cylindrical core geometry is about 4% greater than that of the experimental one.

The strip contact angle and blend cross section will also depend on the blend composition. Fondecave and Brochard Wyart[40] observed a "leak out transition" for a polymer with an oligomer as the solvent. Above a critical polymer concentration, partial wetting is observed whereas below this value the solvent escapes and wets the surrounding region resulting in an encapsulated polymer droplet with a precursor film. For the SAN/PMMA system, this "fried egg" configuration should be stable for PMMA volume fractions of 0.27 or less. On the other hand, if the volume fraction of PMMA is greater than 0.50, the PMMA wetting layer takes a Gaussian shape with a contact angle of at least 8° in order to minimize the system energy.[41] This analysis is consistent with our experimental observations for a blend with a PMMA volume fraction of 0.48 to adopt the final morphology shown in Figure 1.

Phase Evolution. Thin films of SAN/PMMA confined to a narrow strip display distinct morphologies, corresponding to three stages of phase evolution. During the early stage, the near-surface region displays a bicontinuous, interconnected morphology consistent with a spinodal decomposition phase separation mechanism. Phase separation is not yet perturbed by lateral confinement at early times. During the intermediate stage, the SAN-rich matrix becomes encapsulated by the PMMA-rich wetting phase. The matrix contains PMMA-rich minority domains, which grow from the near-surface toward the substrate. Along the edge of the strip, PMMA-rich domains rapidly coarsen, resulting in a thick wetting layer parallel to the strip. During the late stage, the characteristic features are the healing of PMMA-rich domains and, most uniquely, the formation of a SAN-rich core encapsulated by a PMMA-rich shell as anticipated by Figure 1.

To quantify phase evolution during the early, intermediate, and late stages, the number density of PMMA-rich phases and phase size are measured. The number of phases per 100 μm^2, N_d, is determined by AFM analysis (see Figure 5) near the center (flat) region. During the early stage, Figure 6a shows that N_d decreases from 650 to 150 between 1 and 2 h, indicative of rapid coarsening. During the intermediate stage, phase coarsening slows down. For example, N_d only decreases from 30 to 14 between 4 and 20 h, respectively. Because of the large distance between phases in the late stage, the phases are unable to coalesce, and therefore, N_d can only decrease by healing of individual PMMA-rich domains.

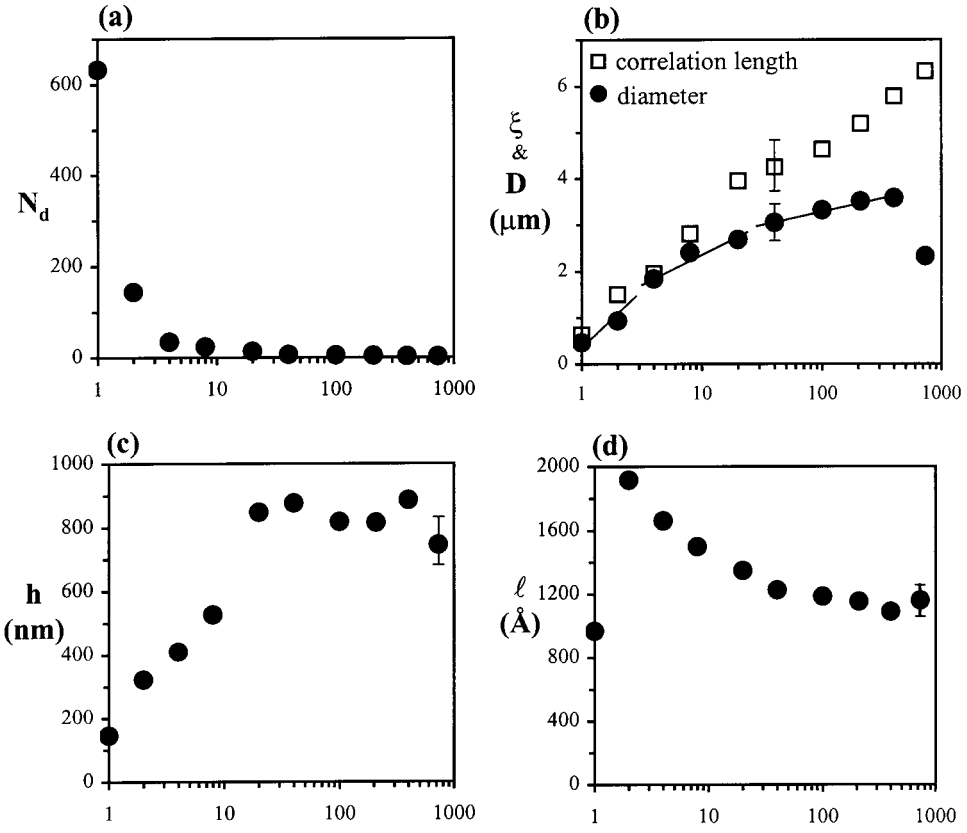

Figure 6. Using AFM analysis from images such as those shown in Figure 5, the PMMA-rich domain (a) number density, N_d, (b) diameter, D, and correlation length, ξ, (c) depth, h, and (d) wetting layer thickness, l, are measured. The parameters are defined in the Experimental Section. Representative error bars are included for D, ξ, h, and l. The solid lines are to guide the eye.

The PMMA-rich domains can be characterized by their diameter, D, the correlation length between phases, ξ, and the depth of the domain in the SAN-rich matrix, h. Figure 6b shows that D and ξ both initially increase rapidly with annealing time. Whereas ξ continues to increase as the logarithm of time, D increases more slowly during intermediate times and even decreases at late times as the PMMA phase begins to shrink. Simultaneous with the growth of D, Figure 6c shows that h increases rapidly at first before reaching the substrate wetting layer after ca. 20 h. This behavior contrasts with previous experiments on semiinfinite films where the PMMA-rich domains are only observed to span the wetting layers. After 732 h, the PMMA domains begin to shrink and, correspondingly, h decreases. From the behavior of D, ξ, and h (Figure 6b,c), we can begin to address the mechanisms of growth for the three stages of evolution.

The *early stage* is characterized by a bicontinuous morphology and rapid phase growth. From the early stage data in Figure 6b,c, both D and h increases rapidly with time to exponents of 1.0 and 1.1, respectively. This rapid phase growth suggests a hydrodynamic flow mechanism in agreement with experiments on semiinfinite films.[26−28,42] Thus, phase growth appears undisturbed by lateral confinement during the early stage. As shown in Figures 4 and 5, the interconnected phase morphology begins to disappear after 4 h. These phases evolve into small domains beneath the wetting layer, as represented by the schematic in Figure 7a.

During the *intermediate stage*, the growth rate of the PMMA-rich domains decreases. Between 4 and 20 h, D and h grow as $t^{0.23}$ and $t^{0.45}$, respectively. To understand this behavior, we apply a diffusion-controlled model to

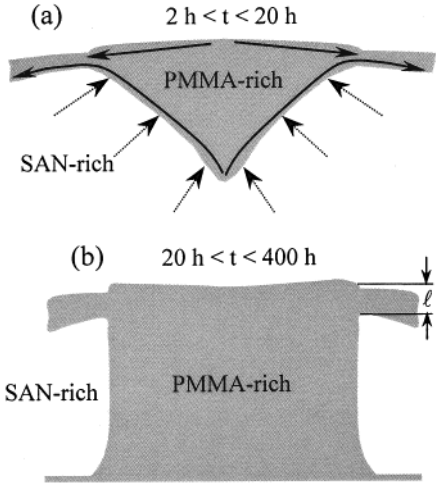

Figure 7. Representation of the PMMA-rich domain during the (a) early intermediate stage and (b) late intermediate and late stages. The gray and white colors represent the PMMA-rich domain and SAN-rich matrix, respectively. The early intermediate stage is characterized by partial penetration of the PMMA-rich domains into the SAN-rich matrix. Although D increases slowly during this time, PMMA flows from the cone-shaped domain into the wetting layer as represented by the solid arrows. The dotted arrows represent the flux of PMMA into the domain. At later times (b), the PMMA-rich domain has fully penetrated the SAN-rich matrix and adopts a disk shape. The growth of D slows down dramatically during this time, and eventually the domains shrink. The wetting layer thickness is denoted by "l".

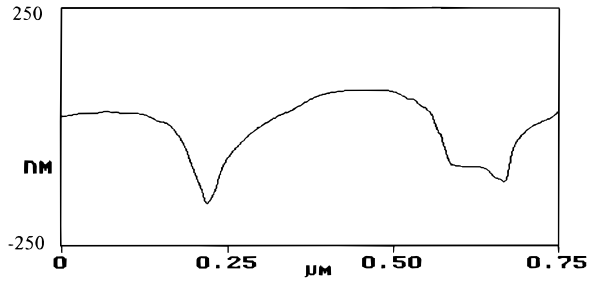

Figure 8. AFM cross section of a smooth (left) and irregular (right) domain after 1 h. The PMMA has been removed.

describe the growth of the cone-shaped domain sketched in Figure 7a. On the basis of this geometry, h and D are related by $h = aD^b$, where a is a constant and b is determined from Figure 6b,c. Because h grows faster than D, b is always greater than 1 during the intermediate stage. Using the geometric relationship and assuming growth by diffusion, the diameter and height are described by $D \propto t^{1/3}$ and $h \propto t^{b/3}$, respectively. These equations likely overestimate the growth rates because the flux of PMMA out of the domain is not included in the model. As indicated by the solid arrows in Figure 7a, this outward flux is driven by the curvature of the PMMA-rich domain. Surface bumps provide direct evidence for this outward flow of PMMA toward the surface. For example, the inset of Figure 4 at 20 h shows a typical surface bump, which is about 25 nm higher than the surrounding area.

Besides diffusion, phase coarsening provides another growth mechanism during the *early* and *late intermediate stages*. There are several reasons to invoke a phase coarsening mechanism. After 4 h, N_d begins to decrease more slowly and, correspondingly, D begins to increase more slowly as shown in parts a and b of Figure 6, respectively. Second, for a domain to grow, the diffusive flux into the domain must be greater than the flux out that is due to hydrodynamic flow. If only diffusion supplied the domain, the net flux should be away from the domain, leading to a reduction in D. Third, Figure 8 shows that the growth front contains smooth (left) and irregular (right) protrusions after removing the PMMA component from a film annealed for 1 h. The protrusions are about 200 nm deep. Protrusions with a high interfacial area may result from incomplete phase coarsening between adjacent domains or between the growing front and an isolated phase within the SAN-rich matrix. Although the former mechanism is obvious from the top-view images in Figure 5, the matrix may contain isolated PMMA-rich domains encapsulated by the SAN-rich phase. Because of confinement, these domains should be much smaller than those originating from the interface between the wetting layer and SAN-rich matrix[4] and therefore readily dissolve into the growing tip by capillary evaporation.

The *late intermediate stage* begins when the PMMA-rich domains reach the wetting layer on the substrate and form a disk as illustrated in Figure 7b. During this stage, D continues to increase although at a continually decreasing rate, $D \sim t^{0.1}$. The slow growth of D is consistent with a decrease in diffusive flux, as each phase approaches their coexisting compositions, and a reduction in the phase coarsening mechanism due to large domain spacing. The growth of D during the late intermediate stage is further complicated by partial back-flow of PMMA from the wetting layer. Because the disk radius exceeds the height, capillary pressure will tend to increase the disk diameter by back-flow of PMMA into the domains. This back-flow is supported by the collapse of the surface bumps on the PMMA wetting layer as shown in the 100 h inset of Figure 4. For semiinfinite films, the collapse of surface bumps leads to back-flow of PMMA from the wetting layer into the domain.[28] However, for the confined strip, the PMMA can flow along the wetting layer toward the edge of the strip, as well as into the domain. The slow growth of D and rapid wetting along the strip edge suggests that back-flow occurs predominantly through the wetting layer.

During the *late stage* of phase evolution, D reaches a maximum value of 3.5 μm at 400 h and then decreases. Even though the exact mechanism is unclear, PMMA domain shrinking is consistent with a reduction of interfacial area. Although data are limited, the rapid healing of the PMMA domains suggests a hydrodynamic flow mechanism. In contrast to the semiinfinite film, the surface of the confined blend remains smooth throughout the entire phase evolution. In the former case, a trilayer A/B/A structure forms parallel to the substrate followed by rupturing of the B interphase due to capillary fluctuations. During the late stage phase evolution in a confined strip, the SAN-rich phase forms a central core encapsulated by a PMMA-rich shell, resulting in a final morphology with the cross section drawn in Figure 1. Both the healing of domains and the core/shell structure suggest that the final morphology is stable.

The stable morphology of the SAN-rich core surrounded by the PMMA-rich shell can be explained using the capillary thread theories developed by Tomotika,[43] Hammond,[44,45] and others.[46,47] Tomotika analyzed the stability of a cylindrical thread of a viscous liquid surrounded by another viscous fluid of infinite size. Following Tomotika, Eleman et al.[43,46] determined the time for a thread to break:

$$t_b = \frac{\eta_c R_0}{\Omega(\lambda,p)\gamma} \ln\left(\frac{1.30\sigma {R_0}^2}{kT}\right) \qquad (1)$$

where η_c, R_0, $\Omega(\lambda,p)$, and γ are the matrix viscosity, the radius of the initial thread, a parameter that depends on the viscosity ratio (p) and capillary wavelength (λ), and the interfacial tension between the fluids, respectively. For the PMMA:SAN system, η_c is the viscosity of PMMA,[48] which is around 5.4×10^5 P at 200 °C, R_0 is estimated to be 2.5 μm according to AFM, the $\Omega(\lambda,p)$ value[47,48] is based on $p = \eta_{SAN}/\eta_{PMMA}$ and is 0.073, and the estimated interfacial tension is 0.52 mJ/m^2. Thus, the time to break the thread turns out to be about 130 h for a SAN thread surrounded by an infinite PMMA medium. In our experiment, the SAN core was stable for annealing times up to 1500 h. One difference between Tomotika's model and our experimental morphology is the finite thickness of the encapsulating medium. Extending Tomotika's study, Hammond analyzed the stability of a thread surrounded by a cylindrical fluid of finite thickness within a pipe. The rate to break the thread was found to decrease as the surrounding layer thickness decreased. Compared to the infinite medium, the time to break increases by a factor of ca. 30 for our system. The viscoelastic nature of polymer and the broad interfacial width are two additional stabilizing influences that are not included by

these models. For these reasons, after forming the core/shell structure, the SAN-rich core is expected to be robust against destabilizing factors, such as capillary fluctuations.

Wetting Layer Thickness. Figure 6d shows that the wetting layer thickness, l, at the air/blend interface initially increases rapidly, decreases at a moderate rate, and then decreases very slowly, approaching 1100 Å. Qualitatively, this behavior is similar to that observed for wetting of a semiinfinite film although the mechanism of thinning is quite different. Figure 6d shows that l increases rapidly to a thickness of 2000 Å within 2 h. Although based on only two values, a growth rate of $l \sim t^1$ is consistent with the hydrodynamic flow mechanism previously observed in semiinfinite films.[27] Similar to the semiinfinite case, the near-surface morphology of the strip shows an interconnected PMMA-rich network, which provides a pathway from the bulk to the surface layer. Thus, at early times, wetting layer growth is independent of lateral confinement.

Throughout the early intermediate stage (2 h $< t <$ 20 h), the wetting layer thins as approximately $l \sim t^{1/6}$. Concurrently, D and h continue to increase as shown in parts b and c of Figure 6, respectively. In the semiinfinite film case, wetting layer thinning takes place by the back-flow of PMMA from the wetting layer into the PMMA-rich domain. During the early intermediate stage, the PMMA-rich domain only partially penetrates the SAN-rich matrix as depicted in Figure 7a. Thus, we propose that the curvature of the PMMA-rich domain produces a capillary pressure, which drives PMMA out of the domain and into the wetting layer as shown by the solid arrows in Figure 7a. If this is an accurate description, how does one explain the thinning of the surface-wetting layer along the center of the strip? Because of the rapid domain coarsening near the strip edges (e.g., 20 h in Figure 5), the wetting layer thickness difference between the center (thin) and edge (thick) produces a pressure gradient. Because of this gradient, PMMA will tend to flow along the surface-wetting layer and toward the edges of the strip as shown in Figure 7a.

After the domain growth front reaches the substrate-wetting layer at 20 h (Figure 5), the wetting layer thickness decreases much more slowly and approaches a value of ca. 1100 Å. During this time, PMMA will tend to flow from the wetting layer into the open domain (Figure 7b) because of capillary pressure (i.e., $P \propto \gamma(2/D - 2/h)$ for $D > h$). PMMA will also continue to flow along the wetting layer toward the edges of the strip. A theoretical model capturing the complex flow behavior of PMMA is presently lacking.

Final Remarks

In this paper, we investigate the dynamics of phase separation in a laterally confined polymer blend thin film and find three stages of evolution. The early stage is characterized by an interconnected morphology and rapid formation of a PMMA-rich wetting layer around the entire strip. The diameter and depth of PMMA-rich domains increase rapidly during this time. Whereas phase separation appears undisturbed by lateral confinement initially, polymer blends display some unique morphological and kinetic signatures during the intermediate and late stages. First, the PMMA-rich phases inside the SAN-rich matrix form cone-shaped domains that grow from the surface to the substrate. Relative to the early stage, the diameter and depth grow at a slower rate. After the PMMA-rich phases touch the wetting layer on the substrate, the domains continue to grow with time even more slowly. Eventually, during the late stage, the PMMA-rich domains heal from the SAN-rich matrix. Second, whereas it increases rapidly during the early stage, the wetting layer at the top of the strip becomes thinner during the intermediate and late stages. In contrast to the semiinfinite case where thinning occurs by back-flow, the flow of PMMA in the strip case is driven by a pressure gradient created by a difference in wetting layer thickness between the center and edge. This gradient produces a flow of PMMA along the surface-wetting layer and toward the edge of the strip where it accumulates throughout the intermediate and late stage. During the late stage, the PMMA-rich domains heal, resulting in a solid SAN-rich core encapsulated by the PMMA-rich wetting layer. The stability of this final morphology contrasts with the behavior of semiinfinite films of similar thickness, which roughen during the late stage of phase separation.

Compared to a semiinfinite film with a uniform thickness, phase separation in a confined strip is relatively complicated because of the variation in film thickness across the strip. In our case, the film thickness ranges from a few hundred angstroms near the edge to more than 1 μm near the center. As a result, the thin and thick regions of the strip may phase separate at different rates and possibly by different mechanisms. In the PMMA:SAN strip, phase separation proceeds most rapidly in the thin region, and as a result PMMA rapidly accumulates along the edge of the strip. At the same time, the SAN-rich phase flows toward the central core, resulting in the stable core/shell morphology drawn in Figure 1. This core/shell phase structure has great potential as a facial route for preparing optical and conducting fibers encapsulated in a protective polymer sheath.

Acknowledgment. We acknowledge primary financial support from the NSF DMR program, Grant No. DMR-99-74366, and partial support and shared experimental facility support from the NSF MRSEC program, Grant No. DMR96-32598. We acknowledge use of the Microfabrication Laboratory at UPenn. We thank Dr. Pen-Cheng Wang, Mr. Marko Radosavljevic, and Mr. Vladimir Dominko for assistance in fabricating the elastomeric molds and Dr. Eric Weeks for helping with the confocal microscope studies. We also thank Mr. Russel Walters, Dr. Howard Wang, and Mr. Marko Radosavljevic for experimental assistance and advice.

References and Notes

(1) Kyu, T.; Saldanha, J. M. *Macromolecules* **1988**, *21*, 1021.
(2) Pan, Q.; Composto, R. J. *Mater. Res. Soc. Symp. Proc.* **1995**, *366*, 27.
(3) Sung, L.; Karim, A.; Douglas, J. F.; Han, C. C. *Phys. Rev. Lett.* **1996**, *76*, 4368.
(4) Kumacheva, E.; Li, L.; Winnik, M. A.; Shinozaki, D. M.; Cheng, P. C. *Langmuir* **1997**, *13*, 2483.
(5) Dalnoki-Veress, K.; Forrest, J. A.; Dutcher, J. R.; *Phys. Rev. E* **1998**, *57*, 5811.
(6) Muller-Buschbaum, P.; O'Neil, S. A.; Affrossman, S.; Stamm, M. *Macromolecules* **1998**, *31*, 5003.
(7) Slep, D.; Asselta, J.; Rafailovich, M. H.; Sokolov, J.; Winesett, D. A.; Smith, A. P.; Ade, H.; Strzhemechny, Y.; Schwarz, S. A.; Sauer, B. B. *Langmuir* **1998**, *14*, 4860.
(8) Gutmann, J. S.; Muller-Buschbaum, P.; Stamm, M. *Faraday Discuss.* **1999**, *112*, 285.

(9) Ade, H.; Winesett, D. A.; Smith, A. P.; Qu, S.; Ge, S.; Sokolov, J.; Rafailovich, M. *Europhys. Lett.* **1999**, *45*, 526.
(10) Zhu, S.; Liu, Y.; Rafailovich, M. H.; Sokolov, J.; Gersappe, D.; Winesett, D. A.; Ade, H. *Nature* **1999**, *400*, 49.
(11) Rouault, Y.; Baschnagel, J.; Binder, K. *J. Stat. Phys.* **1995**, *80*, 1009.
(12) Pereira, G. G.; Wang, J.-S. *J. Chem. Phys.* **1996**, *104*, 5294.
(13) Kerle, T.; Klein, J.; Binder, K. *Phys. Rev. Lett.* **1996**, *77*, 1318.
(14) Fischer, H. P.; Maass, P.; Dieterich, W. *Phys. Rev. Lett.* **1997**, *79*, 893.
(15) Muller, M.; Binder, K. *Macromolecules* **1998**, *31*, 8323.
(16) Binder, K. *J. Non-Equilib. Thermodyn.* **1998**, *23*, 1.
(17) Binder, K.; Puri, S.; Frisch, H. L. *Faraday Discuss.* **1999**, *112*, 103.
(18) Cherrabi, R.; Saout-Elhak, A.; Benhamou, M.; Daoud, M. *J. Chem. Phys.* **1999**, *111*, 8174.
(19) Tanaka, H. *Phys. Rev. Lett.* **1993**, *70*, 53.
(20) Tanaka, H. *Phys. Rev. Lett.* **1993**, *70*, 2770.
(21) Xia, Y.; Whitesides, G. M. *Annu. Rev. Mater. Sci.* **1998**, *28*, 153.
(22) Boltau, M.; Walheim, S.; Mlynek, J.; Krausch, G.; Steiner, U. *Nature* **1998**, *391*, 877.
(23) Karim, A.; Douglas, J. F.; Lee, B. P.; Glotzer, S. C.; Rogers, J. A.; Jackman, R. J.; Amis, E. J.; Whitesides, G. M. *Phys. Rev. E* **1998**, *57*, R6273.
(24) Nisato, G.; Ermi, B. D.; Douglas, J. F.; Karim, A. *Macromolecules* **1999**, *32*, 2356.
(25) Kielhorn, L.; Muthukumar, M. *J. Chem. Phys.* **1999**, *111*, 2259.
(26) Wang, H. Ph.D. Dissertation, University of Pennsylvania, 1999.
(27) Wang, H.; Composto, R. J. *Phys. Rev. E* **2000**, *61*, 1659.
(28) Wang, H.; Composto, R. J. *Europhys. Lett.*, in press.
(29) McMaster, L. P. *Macromolecules* **1973**, *6*, 760.
(30) Suess, M.; Kressler, J.; Kammer, H. W. *Polymer* **1987**, *28*, 957.
(31) Fowler, M. E.; Barlow, J. W.; Paul, D. R. *Polymer* **1987**, *28*, 1177.
(32) Higashida, N.; Kressler, J.; Yukioka, S.; Inoue, T. *Macromolecules* **1992**, *25*, 5259.
(33) Madbouly, S. A.; Ougizawa, T.; Inoue, T. *Macromolecules* **1999**, *32*, 5631.
(34) Unertl, W. N. *Langmuir* **1998**, *14*, 2201.
(35) For a few cases, during molding, residual thin films (~100 nm) were left on the substrate between strips. By comparing strips with and without these residual films, we found that these thin films had little influence on phase separation and wetting.
(36) Using XPS, the surface of an acrylic adhesive peeled from a PDMS elastomer was found to contain silicon, suggesting the transfer of PDMS to the adhesive.
(37) This is the dispersive component of the surface energy for the native oxide covered silicon (Zhao, W.; Rafailovich, M. H.; Sokolov, J.; Fetters, L. J.; Plano, R.; Sanyal, M. K.; Sinha, S. K.; Sauer, B. B. *Phys. Rev. Lett.* **1993**, *70*, 1453).
(38) The calculation of the interfacial energy of PMMA/SAN was based on Hong et al. (Hong, Z.; Shaw, M. T.; Weiss, R. A. *Macromolecules* **1998**, *31*, 6211). The molar fraction of AN in SAN was 0.49.
(39) The surface energy of PMMA was obtained from literature (Brandrup, J.; Immergut, E. H. *Polymer Handbook*, 3rd ed.; John Wiley & Sons: New York, 1989) with a number-average molecular weight of 3000.
(40) Fondecave, R.; Brochard Wyart, F. *Macromolecules* **1998**, *31*, 9305. The amount of PMMA required to produce the "fried egg" configuration was estimated by assuming a 100 nm layer of the PMMA-rich phase, which encapsulated the SAN-rich core. The material was confined in a strip with a height and width of 1.0 μm and 17 μm, respectively. The SAN-rich core was assumed to have the same dimensions as the final morphology of 50/50 blend strip.
(41) The contact angle was estimated from the slope of the line connecting the three-phase contact point and the point at the experiment curve where the second derivative equals zero. The area under this line was used to obtain the new volume fraction of PMMA.
(42) Jandt, K. D.; Heier, J.; Bates, F. S.; Kramer, E. J. *Langmuir* **1996**, *12*, 3716.
(43) Tomotika, S. *Proc. R. Soc. (London)* **1935**, *A150*, 322.
(44) Hammond, P. S. PhD Dissertation, Cambridge University, 1982.
(45) Hammond, P. S. *J. Fluid Mech.* **1983**, *137*, 363.
(46) Elemans, P. H. M.; Jansen, J. M. H.; Meijer, H. E. H. *J. Rheol.* **1990**, *34*, 1311.
(47) Watkins, V. H.; Hobbs, S. Y. *Polymer* **1993**, *34*, 3955.
(48) The viscosity of PMMA was estimated from Fuchs et al. (Fuchs, K.; Friedrich, C.; Weese, J. *Macromolecules* **1996**, *29*, 5893) and scaled with M_w and temperature for a PMMA having a similar tacticity as ours. The viscosity ratio was calculated at a temperature of 185 °C. The ratio at 200 °C should be similar to this value, because the shift factor is similar for both SAN and PMMA.

MA992092M